Toward Combining Speed, Efficiency, Versatility, and Robustness in an Autonomous Quadruped

Marco Hutter, Christian Gehring, Mark A. Höpflinger, Michael Blösch, and Roland Siegwart, *Fellow, IEEE*

***Abstract*—This paper provides an overview about Starl*ETH*: a compliant quadrupedal robot that is designed to study fast, efficient, versatile, and robust locomotion. The platform is driven by highly compliant series elastic actuation, which makes the system fully torque controllable, energetically efficient, and well suited for dynamic maneuvers. Using model-based control strategies, this medium dog-sized machine is capable of various gaits ranging from static walking to dynamic running over challenging terrain. Starl*ETH* is equipped with an onboard PC, batteries, and various sensor equipment that enables enduring autonomous operation. In this paper, we provide an overview about the underlying locomotion control algorithms, outline a real-time control and simulation environment, and conclude the work with a number of experiments to demonstrate the performance of the presented hardware and controllers.**

***Index Terms*—Compliant system, dynamic locomotion, legged robots, quadruped robot, series elastic actuation.**

I. Introduction

RESEARCH in legged robotics currently faces a large push from an increasing demand for machines that can operate in natural environments and support us in our daily tasks. Boosted by recent environmental disasters (e.g., Fukushima 2011), this increasing request is picked up by different large-scale projects supporting the development toward closing the performance gap between robots and their biological counterparts. To this end, we identify four important characteristics that need to be commonly improved: *versatility*, *speed*, *efficiency*, and *robustness*. A novel system should be able to offer different modes of locomotion spanning the range from static climbing to dynamic running. It should be able to robustly interact with the environment and to cope with significant uncertainties or disturbances, while at the same time using only small amount of energy to propel it forward.

A. State of the Art

Analyzing the state of the art of legged platforms and particularly quadrupedal robots shows that current solutions are not able to unite these capabilities in one single machine. The classical robotic devices are built on the strong background of industrial robotic arms. Electrically driven Humanoid (e.g., *Honda's ASIMO* [2], *Toyota's Humanoid* [3], *HRP series* [4]) or quadrupedal machines (e.g., *LittleDog* [5], *ALoF* [6], *TITAN series* [7]) with high gain controllers and large gear ratios impressively demonstrated sophisticated engineering and highly elaborated motion planning and execution. While having a similar appearance and a comparable number of degrees of freedom as the natural counterparts, these systems behave fundamentally different. The stiff, high gain position controlled setup requires very accurate planning and execution, which results in lack of robustness since the robot can barely cope with external disturbances [8]. Although, these deficiencies can be overcome by the integration of appropriate force sensors, such stiff robots are inappropriate for dynamic maneuvers, as high peak loads occurring due to the intermittent ground contact tend to harm the gearboxes and sensors. An interesting and promising approach for reducing these impact effects is to build upon high-torque electric motors such as in *MIT cheetah* [9], which allow us to significantly lower the gearbox reduction and, hence, the reflected inertia. While resulting in great locomotion performance [10], most components do not readily exist in different scales and need to be custom made to a large extent.

The requirement for an impact-robust actuator with a high power to weight ratio [11] makes hydraulic actuators widely used in modern-legged applications. Highly elaborated quadrupedal robots like Boston Dynamic's *BigDog* [12] and *LS3* [13], or the research platform *HyQ* [14], are hydraulically actuated similar to some of the most advanced humanoid robots developed by Sarcos, Inc., or Boston dynamics. While these heavy, huge, and bulky systems clearly benchmark the state of the art in terms of *versatility*, *robustness*, and *speed*, they are highly inefficient from an energetic point of view and difficult to handle respectively downsize. Estimations based on experimental data available for *BigDog* resulted in a (dimensionless) cost of transport (COT) [15] of about 15 [16], which is less efficient than the electrically actuated *ASIMO* (3.2; see [17]) and about 50 times worse than a human (0.3; see [18]).

The energetic efficiency found in nature can be attributed to a large extent to the exploitation of passive pendulum- and spring dynamics [19]. The pendulum motion supports the swing leg phase while walking. This was adapted in the so-called passive dynamic walkers [20] and was lately extensively exploited when the Cornell Ranger was setting the world record with respect to a low COT [21]. Passive spring dynamics, on the other hand, evolve due to compliant elements in muscles and tendons that allow mechanical storage of potential energy after

Manuscript received March 4, 2014; accepted September 22, 2014. Date of publication October 20, 2014; date of current version December 3, 2014. This paper was recommended for publication by Associate Editor P. Soueres and Editor A. Kheddar upon evaluation of this reviewer's comments. Part of this work was published in [1]. This work was supported in part by the Swiss National Science Foundation through the National Centre of Competence in Research Robotics, as well as by the Hans Eggenberger Foundation.

The authors are with the Autonomous Systems Lab, Institute of Robotics and Intelligent Systems, ETH Zurich, Zurich 8092, Switzerland (e-mail: mahutter@ethz.ch; gehrinch@ethz.ch; markho@ethz.ch; bloeschm@ethz.ch; rsiegwart@ethz.ch).

Color versions of one or more of the figures in this paper are available online at http://ieeexplore.ieee.org.

Digital Object Identifier 10.1109/TRO.2014.2360493

landing and to release it again before lift-off [22], [23]. These findings initiated a fundamental shift in the development of robotic systems suited for dynamic maneuvers away from the classical paradigm "the stiffer, the better." Motivated by Raibert's seminal research on hopping robots with pneumatic pistons [24], researchers employed mechanical compliance in various configurations to enable dynamic gaits. Depending on the particular design, springs are integrated directly in prismatic legs [25]–[27] or in the knee and ankle joints of articulated designs [28]–[35]. In all these robots, motion emerges to a large extent passively from the mechanical dynamics and the actuators are merely used to shape the motion and to compensate for friction and impact losses. Similar approaches were also used to develop quadrupedal robots of different scale such as KOLT [36], Scout series [37], Tekken series [38], Cheetah-Cub [39], or Puppy series [40]. Like the single legs, these more complex systems use the springs to absorb impact shocks at landing, as well as to enable dynamic gaits by means of temporary energy storage.

Compliant elements are not only used to enable and support dynamic locomotion. Based on work done by Pratt and Williamson [41], people started to use the so-called series elastic actuators (SEA) for high fidelity force control [42]. To this end, spring deflection is measured using position encoders and actively controlled to achieve the desired torque output. The advantages of impact robustness and force/torque controllability motivated different groups to realize these ideas in bipedal platforms like *HUME* [43], *BIOBIPED* [44], *COMAN* [45] or M2V2 [46]. In comparison with hydraulic systems, electrical SEAs are built upon widely available components and are easily downscalable, simple, and clean to handle in any lab environment. Due to their mechanical softness in terms of backdrivability and low system inertia, these systems are perfectly suited to continuously interact with their environment. They can cope with (unexpected) ground contact collisions and are, at the same time inherently, safe for hand-in-hand collaboration with human operators. However, since the springs act as a mechanical low-pass filter, the closed-loop control bandwidth significantly drops in comparison with rigidly actuated devices and requires a careful design of the overall control strategy.

The transition from classical walking machines [47] to such compliant systems comes along with a paradigm shift from traditional and well-elaborated position control approaches to novel torque control-based strategies. Thereby, the ongoing improvement in computational power allows the integration of increasingly complex model-based controllers. This ranges from intuitive virtual model approaches [48] to powerful inverse dynamics methods for floating base systems [49]–[52]. In addition to stabilizing the motion of complex robotic systems, these approaches allow simultaneous optimization of the interaction forces and are, hence, perfectly suited to make legged systems robustly operate in natural environments.

B. Contribution

Toward combining the advantages of *versatility*, *speed*, *efficiency*, and *robustness* in one single device, we developed the Springy Tetrapod with Articulated Robotic Legs (Starl*ETH*), which pushes the state of the art in the field of autonomous electrically actuated quadrupeds (See Fig. 1). The system has the size of a medium dog: With a body length of about 0.5 m and a total mass of about 25 kg, it can be easily handled by a single operator. This robot is fully actuated [12 degrees of freedom (DoF)] by highly compliant SEAs that allow for precise joint torque control and substantial energy storage. At the same time, the mechanical compliance ensures robustness for ground contact interaction, as the spring decouples the gearbox from the link.

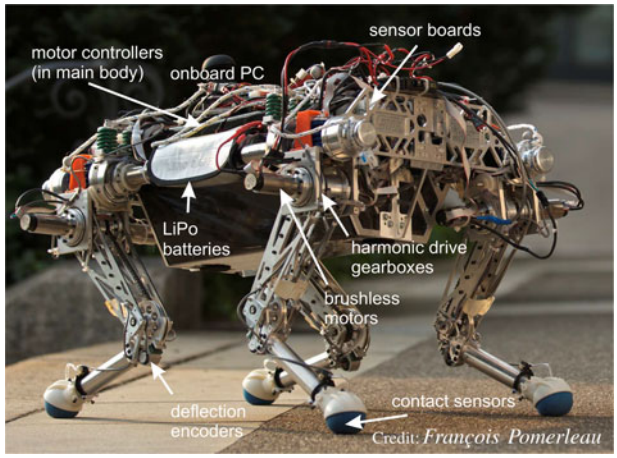

Fig. 1. Starl*ETH*: a compliant quadruped developed for *versatile*, *fast*, *efficient*, and *robust* locomotion.

The contribution of this paper is manifold and can be seen as a research overview about *designing*, *integrating*, and *controlling* a compliant quadrupedal platform. We introduce the hardware prototype, which is based on earlier studies conducted on a single leg [53]. Thereby, important design considerations and different system performance specifications are discussed and experimentally validated. We address the setup of a real-time simulation and control environment and show how a proper integration of software and hardware can lead to a powerful tool for development. Given the full torque control capability of Starl*ETH*, we outline a tool chain to achieve sophisticated locomotion. This includes *behavior generation*, *behavior control*, and *low-level joint control*. Starl*ETH* has the ability to exploit different gaits ranging from static walking to dynamic running including full air phases. These gaits are continuously adapted with smooth transitions depending on the desired running speed. Experiments were conducted with a locomotion velocity of up to 0.7 m/s that corresponds to more than 1.5 body lengths per second and a Froude number of 0.15. We outline torque-based control approaches to robustly stabilize these gaits in case of external disturbances such as unobserved obstacles to external pushes. Building upon the high efficiency and energy preserving mechanisms in the springs, Starl*ETH* is capable of autonomous long distance (>1 km) trotting with a power autonomy of more than 1 h . We analyze in detail the energy consumption for the individual components, as well as for the entire system. For dynamic gaits, the robot requires in average less than 230 W total power, which corresponds to an overall COT of 1.7. The extensive experimental section is illustrated with a movie,[1] and the individual segments are listed in Table III in the Appendix.

[1] http://youtu.be/4ZbifH0Mv4w.

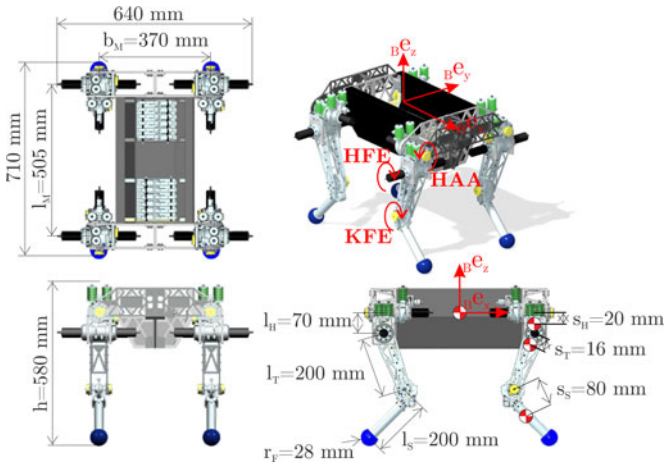

Fig. 2. Kinematic structure and dimensions of Starl*ETH* adapted from [1].

TABLE I
SPECIFICATIONS OF STARL*ETH* IN ADDITION TO FIG. 2

total mass	25	kg	max./min. $\varphi_{j,\mathrm{HAA}}$	$-60/60$	$^\circ$
- m_M (body)	13	kg	max./min. $\varphi_{j,\mathrm{HFE}}$	$-80/80$	$^\circ$
- m_H (hip)	0.6	kg	max./min. $\varphi_{j,\mathrm{KFE}}$	$-175/60$	$^\circ$
- m_T (thigh)	1.56	kg	max. joint torque	30	Nm
- m_S (shank)	0.32	kg	max. joint speed	600	$\frac{^\circ}{s}$
max payload[a]	25	kg			

[a]see Section V-A.

C. Structure of the Paper

This paper will first address the ideas and design principles behind Starl*ETH*. We elaborate the considerations about the mechanical design, the underlying actuation concept, as well as the electronics and software environment. In the following, we give a brief overview about the applied control principles and appropriately refer the interested reader to the relevant literature. This is followed by an extensive experimental part where we evaluate the system-, actuator-, and control performances, as well as by a final discussion and comparison with other existing devices.

II. HARDWARE DESCRIPTION

This section describes the mechanical structure, the underlying actuation principles, as well as the sensor and electronic components of Starl*ETH*.

A. Mechanical Structure

Starl*ETH* features four identical, completely symmetric articulated legs connected to a single rigid main body. With a body length of about 0.5 m, segment lengths of 0.2 m, and a total weight of 25 kg, this robot has the dimension of a medium-sized dog (see Fig. 2 and Table I). The main body is manufactured as a monocoque based on a carbon-fiber sandwich structure with aluminum front- and back connectors. The high stiffness guarantees minimal (unobservable) body deflections with a total weight of less than 2 kg. It contains well-protected, all-electronic parts, such as motor controllers and sensor boards. At the same time, the tolerances for the attachment of the hip abduction drive unit can be satisfied through the aluminum construction.

The conceptual leg design is based on earlier studies that we conducted to optimize a planar running leg [53]. In the development of the mechanical structure of these legs, we put emphasis on keeping the inertia of the moving segments minimal. This was achieved by a dense integration and a lightweight construction based on high tensile aluminum. All actuators are concentrated at the main body through the use of chain and cable pulley transmissions. This is beneficial to ensure fast swing leg motion and to reduce impact losses at the intermittent ground contact.

All legs and segments are built in a completely symmetric way with modular interfaces at the hip, as well as at the knee joint. This allows to quickly (<5 min) exchange the shank and thigh elements as required to replace certain elements or to change the leg configuration. Although, there exist different studies indicating that the most common *X-configuration* is best suited for quadruped robots (for a detailed discussion, see [54, ch. 3.2.4]), there is no clear evidence on this. Fig. 4 shows some possible leg configurations of Starl*ETH*, whereby exactly the same parts are used in any of them: the default *X-configuration*, the *O-configuration*, the mammalian *M-configuration*, and the unusual *OX-configuration*. As it will be outlined in Section IV, we designed all our controllers fully model based. This allows to run the locomotion controller with exactly the same parameters on any of these configurations. While a detailed differentiation is beyond the scope of this paper, a set of trotting experiments with these different configurations can be found in movie segment 2.

B. Actuation Design

Starl*ETH* is driven by *Maxon EC-4pole brushless (BLDC)* 200 W motors and *Harmonic Drive (HD) CSG-14* gearboxes with a 1:100 reduction. The choice for the components was mainly driven by the availability of high-performance gearbox, drive, and motor control units, whereby the power to weight ratio was optimized. HD gearboxes are clearly favorable due to their low size and weight and since they work backlash-free. The decisive factor for the choice of the Maxon BLDC motor was the high dynamic performance (low rotor inertia) and high specific power. We tested several components such as comparable dc (Maxon RE35) or flat motors with higher output torque (Maxon EC-flat 60), both of which resulted in significantly lower control performance. The resulting size appears to match scaling rules presented in [56].

The key elements of Starl*ETH* are the highly compliant SEAs that are implemented in all joints using linear compression springs in an antagonistic respectively precompressed setup (see Fig. 3). The compliant elements decouple the motor and gearbox from the joint. This setup ensures robustness against impacts, allows for energy storage to improve the efficiency, and provides full torque controllability. As illustrated in Fig. 3 and in an animation movie[2] of the whole design, we exploit different

[2]http://youtu.be/ByT5xWJlZ8k.

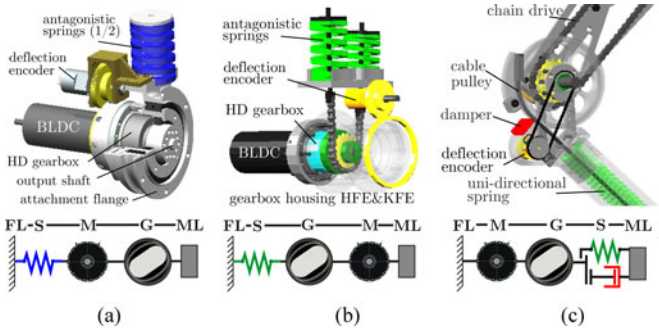

Fig. 3. Three SEA for Starl*ETH* adapted from [55] with a simplified schematics of their functionality: HAA is rigidly attached to the main body (a). The KFE motor and gearbox (not depicted) are integrated in the mirrored drive unit of HFE (b) with the chain drive connecting to the knee joint (c). The joint gearbox housing itself holds as the hip axis.

arrangements of the motor, gearbox, and spring between the fixed link and the moving link.

The knee flexion/extension (KFE) [see Fig. 3(c)] concept was implemented as traditional SEA configuration with the spring between the gearbox output and the knee joint axis. This setup was chosen since the inertia of the most distal link (shank) has the largest influence on impact losses and the swing leg performance. To further reduce the overall leg inertia, the KFE motor and gearbox are located in the hip axis and connected through a miniature chain drive to the knee joint. A chain drive was chosen since, in contrast with a belt setup, it can transmit large torque at low speed. Because the load direction at the knee joint is unidirectional during support phase, the KFE SEA was coupled with a damper (SDA) (see Fig. 3(c), red). This SDA is only active in case of negative load, respectively only during flight phase. A detailed discussion on this methodology and its implications can be found in [53]. As the knee joint is the main contributor to the passive oscillation dynamics of the entire system in ground contact, the stiffness of 36 Nm/rad was chosen to maximally support the passive energy storage and release capabilities during stance phase. The value is based on simultaneous spring parameters and motion optimization for simplified models, which indicates that the choice of mechanical stiffness has a minor influence on the COT but increases the required peak motor power for high stiffness [57]. Using a lumped inertia θ_l of a quarter of the entire body mass, the selected spring results in a natural oscillation frequency of about $f = \frac{1}{2\pi}\sqrt{\frac{k}{\theta_l}} = \frac{1}{2\pi}\sqrt{\frac{k}{1/4 m_{\mathrm{tot}} l_T^2}} = 2\,\mathrm{Hz}$, which is similar to values that can be found in animal or human locomotion [58] and which was experimentally verified in single-legged locomotion [53].

For hip abduction/adduction (HAA) [see, Fig. 3(a)] and hip flexion/extension (HFE) [see Fig. 3(b)], we implemented a so-called reactive setup [59] with motor and gearbox connected to the moving link and the spring to the fixed respectively predecessor link. This has the advantage that springs can be "remotely" mounted and the design can be made more compact. We implement this through antagonistically precompressed springs in combination with a cable pulley [HAA, 3 mm steel, Fig. 3(a)] or chain drive [HFE, 6 mm pitch, Fig. 3(b)]. As a drawback, the mass of the moved link is increased due to the rigidly attached motor. However, since both motors are placed directly on or, in case of HFE, in the rotation axis, the contribution to the segment inertia remains small. The spring stiffness of 70 Nm/rad for HFE respectively 100 Nm/rad for HAA are linearly scaled as a function of the knee joint stiffness and segment lengths such that an external load at the foot point results in similar deflections in all joints and hence to a similar passive compliance. Stiffer springs for HAA and HFE naturally lead to higher closed-loop torque control bandwidth [60] such that the contact force control performance is dominated, respectively limited by the KFE actuator. Furthermore, we ensured and experimentally validated that the closed-loop control bandwidth for HAA and HFE is higher than the unloaded leg oscillation frequency such that passive mass-spring oscillations can be actively damped out (see Section IV-C2).

The springs in all actuators can freely move such that they show a high linearity in stiffness (regression coefficients $R > 0.999$ and mean absolute errors $\overline{|e|} < 0.08\,\mathrm{Nm}$) with minimal friction and damping [53]. Since the choice of stiffness might differ depending on the application or optimization objective, we selected a series of springs (bordignon, ISO10243) that provide equal design dimension (outer diameter) with different stiffness. This offers a simple mean to change the mechanical stiffness of each actuator without adapting the design.

The actuators are designed to deliver about 30-Nm peak torque with a maximal turning speed of more than $600\,^\circ/\mathrm{s}$. The applied *Maxon EC-4pole brushless* motor can simultaneously provide maximal velocity and torque for periodic short-term operation [61]. We put attention on ensuring a large range of motion. Measured from the extended leg pointing along the vertical axis ($\varphi_{\mathrm{HAA}} = \varphi_{\mathrm{HFE}} = \varphi_{\mathrm{KFE}} = 0\,^\circ$), KFE has a bending angle of $[-175°; +60°]$ that allows full extension and retraction of the leg while HFE shows a large swing angle ($[-80°; +80\,°]$). Due to cabling, HAA is currently limited to a range of $[-60°; +60°]$.

C. Sensor and Electronics Equipment

All joint angles and spring deflections, as well as the motor angles are precisely measured by incremental quadrature encoders (AVAGO AEDA3300 with 80 000 counts per revolution respectively AVAGO HEDL with 2000 counts per revolution at the motor). These sensor signals provide full joint state feedback and, in combination with an identified spring characteristic, enable joint position and torque control. Since position measures are only incremental, Starl*ETH* must be homed at startup. Therefore, all four legs are fully retracted to well-defined end stops to initialize the absolute positions and to zero spring deflections before turning the motors ON. A *Xsens MTi* inertial measurement unit (IMU) attached to the main body provides accurate information about body accelerations and rotation rates. To detect ground contact, differential pressure sensors (Freescale Semiconductor Silicon Pressure Sensor MPXV5004) are incorporated with sealed, air-filled racquet balls as tactile foot elements. Thereby, tiny pressure changes in the ball are registered and used to reliably determine the current contact situation. This sensor returns only an amplitude value for the overall contact force. In return,

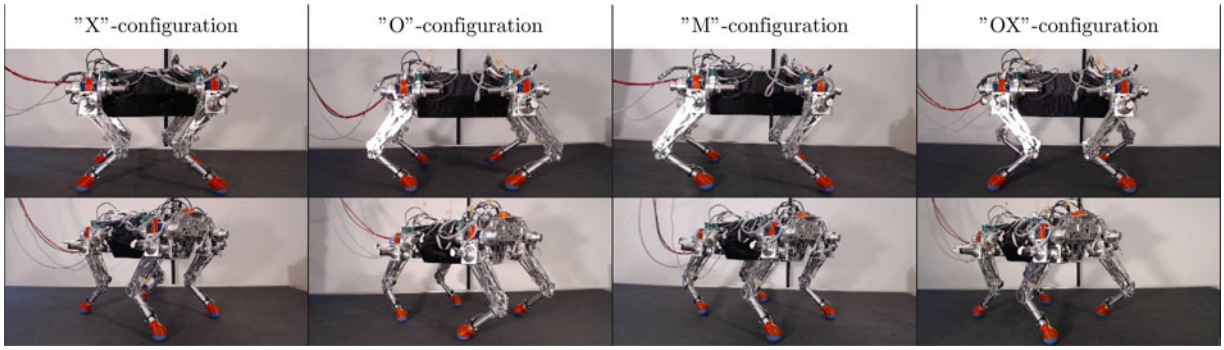

Fig. 4. Starl*ETH* can be operated with different leg configurations (as illustrated in movie segment 2).

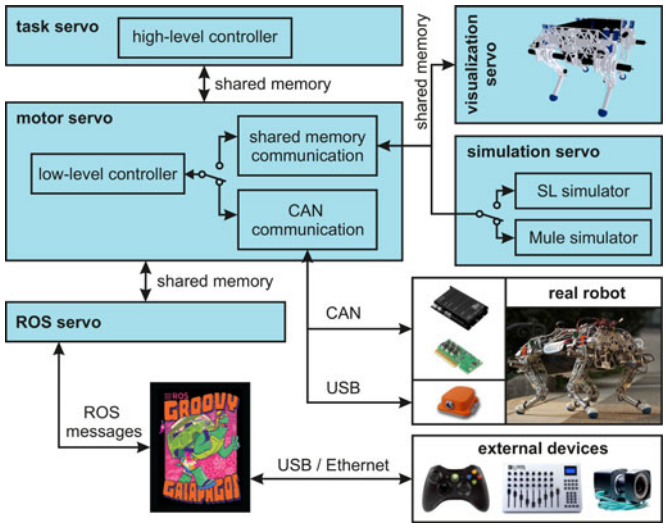

Fig. 5. Real-time simulation and control environment is based on SL [62] combined with analytical global kinematics and dynamics. The framework allows an immediate switch between simulation and actual robot by changing the communication, as well as a direct integration into ROS.

the weight-optimized design (total foot weight is about 70 g) is very robust against impacts and additionally provides useful damping at the point of contact.

For autonomous operation, Starl*ETH* is equipped with an onboard computer (ASUS P8H61 Motherboard, Intel Core i3-2120T processor) that runs the entire control and simulation software (see Section III). The computer communicates via four parallel CAN bus systems (PEAK-System, PCCAN-PCI Express card) with the individual *Maxon EPOS2 70/10* motor controllers. LiPo batteries (1.5 kg , 5 Ah , 44.2 V nominal) deliver power for about 1-h operation time.

III. Software Environment

Controlling complex and inherently unstable systems like Starl*ETH* with 12 actuated joints and 6 unactuated (floating base) degrees of freedom in an often unknown environment requires a powerful and reliable control setup. We realized a framework as depicted in Fig. 5. The setup is based on a single central computer that is responsible for the high-level control part. The software contains a C++ real-time simulation and control environment (SL [62]) running on Ubuntu Linux 13.04 with a low-latency kernel. SL is used as a multibody dynamics engine, for visualization of the robot and its environment, as well as for handling the internal messaging between the different processes through shared memory. It additionally provides tools for data logging and postprocessing.

As a core element, the *motor servo* thread is responsible for timing and coordination of the individual actuators. It contains all low-level regulators (position, velocity, torque) and signal filters. Using either shared memory to access the simulation, or a CAN gateway to communicate with the actual robot, the user has the possibility to run simulations and experiments (even in parallel) with exactly the same controller implementation. This is advantageous for controller development, since it avoids code reimplementation, simplifies debugging and testing, and ensures certain safety if the controllers show good robustness in the simulation.

The *ROS servo* provides an interface to the *robotic operation system*[3] that cannot meet the hard real-time constraints of SL itself. This connection opens the door to a huge set of existing interfaces to different sensors and software packages. In our current setup, this includes a Microsoft Kinect sensor, as well as several external devices such as a gamepad, 3-D joystick, or a slider board using a MIDI interface to steer the robot. It additionally connects to an *OptiTrack* motion capture system with eight cameras (*S250e*). This is used for evaluation and to adjust the speed of the custom made treadmill used for experiments (dimension 2.90 m × 1.60 m) (for details see [63]).

Finally, the *task servo* includes all high-level control, state-estimation, and motion planning tools. To completely decouple it from the multibody simulation, an analytical implementation of the global system kinematics and dynamics of the robot is implemented. To this end, we developed the open-source tool proNEu [64], a MATLAB framework that uses the Symbolic Math toolbox[4] to translate a relative kinematic tree into global kinematics using Euler rotations, and to derive the system dynamics using projected Newton–Euler equations. The state estimator that is implemented on top of the robot model fuses kinematic information with the IMU sensor signals. It is

[3]www.ros.org.
[4]www.mathworks.com/products/symbolic.

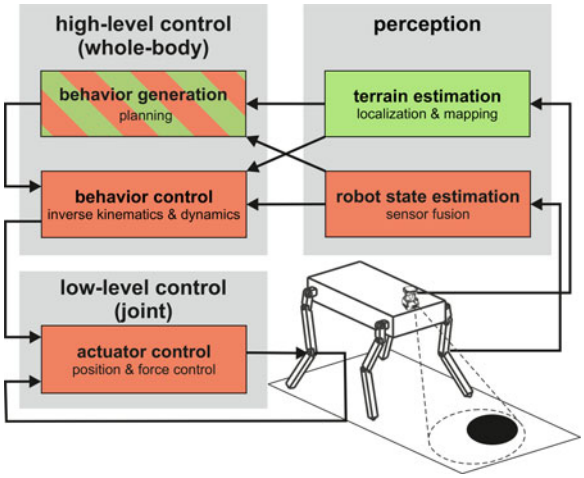

Fig. 6. Locomotion control is considered as a three-step approach, which includes behavior generation, robot stabilization, and low-level control. Real-time critical elements are marked in red.

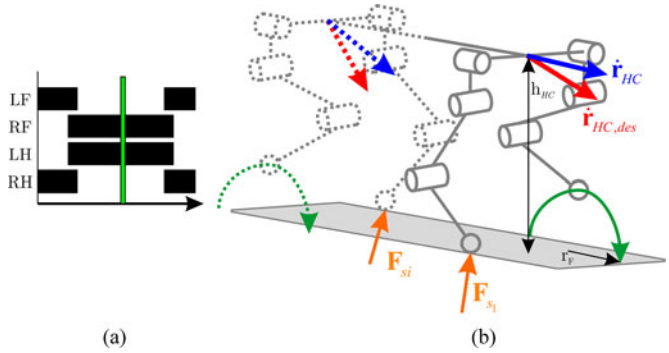

Fig. 7. Timing of the contact points for every gait is defined by a gait graph (a) and the swing foot is positioned as a function of the speed at the corresponding hip reference frame (b) to maintain balance.

based on an extended Kalman filter [65], [66] and estimates not only the base coordinates but is also able to generate a sparse ground elevation map by registering the feet in ground contact. In addition to speed and simplicity of the implementation, this separation between the model used in the controller and the simulation has the benefit that robustness against modeling errors, sensor noise, and imperfect state estimation can already be evaluated in simulation. For simulation, we can either use the integrated ODE-based simulator of SL or a custom made hard contact simulation environment based on Moreau's time stepping algorithms [67].

In practice, the rate-limiting factor in our framework is the data connection of the CAN bus system between the central computer and the motor controllers. Although, we parallelized four channels (1 per leg), the bit rate of $1\,\mathrm{MBits/s}$ limits the overall loop cycle time to about 400 Hz. To resolve this issue, the electronics of a future design will be based upon EtherCAT or a comparable communication system.

IV. Locomotion Control

In this section, we give a brief outline about different control concepts that find its application in controlling Starl*ETH* both for static walking and dynamic running. Although, this is not the main focus of the paper, we would like to foster the comprehension of the experimental section and point the interested reader to the appropriate references. In contrast with traditional work with legged systems investigating foot point and joint trajectory planning and execution [47], our main contribution lies in torque control principles to regulate robust and highly dynamic maneuvers.

Locomotion control, in general, can be considered as a three-step approach (see Fig. 6, left). First of all, motion objectives respectively the entire behavior of the whole-body system needs to be generated (*behavior generation*; see Section IV-A), which involves the selection of appropriate gaits, footholds, main body motion, and contact force or join torque distribution. Second, the desired motion needs to be stabilized using high-level feedback controllers that transform the actual estimated robot state and desired behavior into desired joint-level signals such as position or torque commands (*behavior control*; see Section IV-B). Finally, fast control loops on joint level adjust the motor input to track the set values as accurately as possible (*joint control*; see Section IV-C). While the low-level controller is only depending on local joint feedback, there is large cross coupling between the real time critical (red) and not critical (green) modules of the perception and control branch (see Fig. 6).

A. Behavior Generation

We distinguish between two fundamentally different approaches for motion generation. In rough terrain, the sparsely available foothold locations mainly determine how the main body is moving, i.e., the foothold locations and the motion of the main body are usually planned several stride phases ahead. In that case, *static gaits* are preferred. They guarantee stability at any point of time since the projected center of gravity always lies within the support polygon defined by the footholds. When it comes to less challenging terrain, locomotion speed can be increased and the robot can transition to *dynamic gaits*. Thereby, the foothold locations are chosen to keep balance and to move the system forward.

1) Static Gaits: For the presented experiments, we use a basic trajectory planner both for the main body motion as well as for the foothold locations. The robot continuously executes the stereotypic footfall pattern [68] left-hind (LH), left-front (LF), right-hind (RH), right-front (RF). The trajectory of the main body is optimized two successive steps ahead to minimize the body motion, while guaranteeing a certain safety margin defined as distance between base and support polygon. Research done in the littleDog project [e.g., 69] impressively showed how such an approach can be pushed to the limits to make the robot highly versatile and capable of locomoting in challenging terrain.

2) Dynamic Gaits: Dynamic gaits are to a large extent defined by the footfall pattern and the duration of the gait cycle. In our approach, a gait graph [see Fig. 7(a)] explicitly defines the role of each leg at any moment in time. Legs that are in swing mode need to safely reach the next foothold location to

ensure that the robot can move at the desired speed or to recover balance.

As indicated in Fig. 7(b), the desired stepping locations are calculated similarly to [24] and [70] by

$$\mathbf{r}_F = k_p^{FB}\left(\dot{\mathbf{r}}_{HC,\mathrm{des}} - \dot{\mathbf{r}}_{HC}\right)\sqrt{\frac{h_{HC}}{g}} + k_p^{FF}\left(\frac{1}{2}\dot{\mathbf{r}}_{HC,\mathrm{des}}\Delta t_s\right) \tag{1}$$

with the feedback gain $k_p^{FB} < 0$, the desired velocity $\dot{\mathbf{r}}_{HC,\mathrm{des}}$, the reference velocity $\dot{\mathbf{r}}_{HC}$ at the middle of the front respectively rear hip locations, the hip height h_{HC} above ground, as well as the feedforward gain $k_p^{FF} > 0$, and the corresponding stance duration Δt_s. Furthermore, roll and pitch orientations of the main body are usually kept constant, the heading is adjusted by the desired locomotion direction of the robot, and the desired forward and sideward locomotion speed are taken as higher level (user) input. In most gaits such as low-speed trotting, the body is kept at constant height. For more dynamic gaits like running trot or pronking, a vertical (periodic) oscillation is superimposed. For detailed information about the motion generator for dynamic gaits, the reader is referred to [71], [72].

B. Behavior Control

To realize a desired motion under external disturbances, we adopt two different control techniques that output desired joint torques to adjust the interaction forces $\mathbf{F}_{s_i}$ of all legs in ground contact accordingly [see Fig. 7(b)]. The first method uses virtual force control in combination with Jacobian transposed mapping [48] that was extended for quadrupedal walking [72], and augmented with an optimal force distribution [71]. The second method makes use of prioritized task-space inverse dynamics of floating base systems [73].

1) Virtual Force and Jacobian Transposed Control: The basic idea of virtual force control is to virtually apply forces $\mathbf{F}_{v_i}$ at the robot to achieve the desired motion objectives, for instance, by a simple PD law that represents a virtual spring-damper system between the current and desired pose

$$\mathbf{F}_{v_i} = \mathbf{k}_p\left(\mathbf{r}_{i,des} - \mathbf{r}_i\right) + \mathbf{k}_d\left(\dot{\mathbf{r}}_{i,des} - \dot{\mathbf{r}}_i\right). \tag{2}$$

These virtual forces acting at the main body can only be generated by the stance legs respectively the contact forces $\mathbf{F}_{s_i}$. Hence, the n contact forces must result from the static force/torque equilibrium of the entire system

$$\begin{pmatrix}\mathbf{F}_{s_1}\\ \vdots \\ \mathbf{F}_{s_n}\end{pmatrix} = \begin{bmatrix}\mathbf{I}\ldots\mathbf{I}\\ \tilde{\mathbf{r}}_{s_1}\ldots\tilde{\mathbf{r}}_{s_n}\end{bmatrix}^{+}\begin{bmatrix}\sum\mathbf{F}_{g_i} - \sum\mathbf{F}_{vi}\\ \sum\mathbf{r}_{g_i}\times\mathbf{F}_{g_i} - \sum\mathbf{r}_{vi}\times\mathbf{F}_{vi}\end{bmatrix} \tag{3}$$

with the gravitational forces $\mathbf{F}_{g_i}$ and the cross-product matrix $\tilde{\mathbf{r}}_{s_1}$ of the vector $\mathbf{r}_{s_1}$. Since the unilateral frictional contact does not allow for arbitrary contact forces $\mathbf{F}_{s_i}$, we distribute the net force and torque vectors to the stance legs using a convex optimization that takes into account the contact constraints $F_{s_i}^{\mathrm{tang}} < \mu F_{s_i}^{\mathrm{normal}}$. Finally, the contact forces are mapped to the joint torques using the Jacobian transposed method

$$\boldsymbol{\tau} = -\sum_j \mathbf{J}_{bg_i}^T\mathbf{F}_{g_i} + \sum_i \mathbf{J}_{bv_i}^T\mathbf{F}_{v_i} + \sum_j \mathbf{J}_{bs_i}^T\mathbf{F}_{s_i}. \tag{4}$$

2) Hierarchical Task-Space Inverse Dynamics: In contrast with virtual force control, which is a static method, hierarchical operational-space control strategies account for the full robot dynamics. To this end, achieving a desired task space dynamics (acceleration at specific points), or optimizing the joint torque and contact force distribution can be written as least-squares (LS) problems of different priorities

$$\min_{\mathbf{x}} \quad \|\mathbf{J}\ddot{\mathbf{q}} + \dot{\mathbf{J}}\dot{\mathbf{q}} - \ddot{\mathbf{r}}_{i,\mathrm{des}}\|_2 \tag{5}$$

$$\min_{\mathbf{x}} \quad \|\mathbf{W}_{i,\tau}\left(\boldsymbol{\tau}_i - \boldsymbol{\tau}_{i,\mathrm{des}}\right)\|_2 \tag{6}$$

$$\min_{\mathbf{x}} \quad \|\mathbf{W}_{i,\tau}\left(\mathbf{F}_{s_i} - \mathbf{F}_{s_i,\mathrm{des}}\right)\|_2 \tag{7}$$

with the stacked optimization vector $\mathbf{x} = \begin{pmatrix}\ddot{\mathbf{q}}^T & \boldsymbol{\tau}^T & \mathbf{F}_s^T\end{pmatrix}^T$ of generalized accelerations $\ddot{\mathbf{q}}$, joint torques $\boldsymbol{\tau}$, and contact forces $\mathbf{F}_s$. Additionally, the system dynamics

$$\mathbf{M}\ddot{\mathbf{q}} + \mathbf{b} + \mathbf{g} + \mathbf{J}_s^T\mathbf{F}_s = \mathbf{S}^T\boldsymbol{\tau} \tag{8}$$

with the mass matrix $\mathbf{M}$, Coriolis and centrifugal components $\mathbf{b}$, gravitational part $\mathbf{g}$, support Jacobian $\mathbf{J}_s$, and actuator selection matrix $\mathbf{S}^T$ must to be fulfilled. This constrained prioritized LS problem can be solved using numerical solvers for constrained quadratic programs (e.g., [74]) or an iterative analytical solution [63]. The particular case of controlling Starl*ETH* involves the following motion tasks with decreasing priority: ensuring support constraint, controlling main body height (w.r.t. world), main body pitch and roll angle (w.r.t. body), main body turning rate (w.r.t. world), and main body velocity (w.r.t. body). The expression of the individual tasks in different coordinate systems (w.r.t. world and body) ensures both a simple controller gain tuning and intuitive steering for the user. Furthermore, depending on the contact situation, contact redundancy respectively internal force directions allow for an optimization of the torque or contact force distribution. This is used in our framework to increase the actuator efficiency, as well as to reduce the risk of slippage at the contact points [73].

C. Joint Control

The individual joint actuators are either operated in torque control mode to accurately shape the contact force during stance phase, or in position control mode to fast and precisely regulate the foot position during swing phase. Switching among the different control setups is triggered by contact force measurements.

1) Torque Control: During stance phase, the heavy base and the nonmoving contact constraints allow to approximate the actuator as depicted in Fig. 8(a). This simplification allows to design the joint torque controller independent of the robot respectively the output model. Similar to [75], we rely on a fast low-level velocity control loop of the motor output shaft to compensate for gearbox inertia and friction effects. The velocity controlled motor can be idealized as an integrator and the torque respectively spring deflection PID feedback loop is

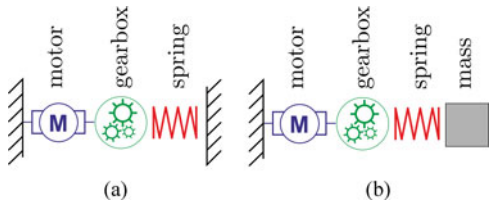

Fig. 8. The high output load model (a) is a good approximation during contact interaction, while the low-output mass model (b) describes the behavior of the free swinging leg.

implemented in a cascaded structure. With this control setup, a bandwidth of about 28 Hz for low amplitudes and about 11 Hz for large amplitudes is achieved with a blocked output. To improve the disturbance rejection and to ensure high-performance torque tracking while the output is moving, the measured joint velocity (velocity of the output mass) is additionally used as a feed-forward compensator. It can be shown that this control loop is *stable* and *passive*, which ensures stability when interacting with the environment [76].

2) Position Control: During swing phase, the SEA can be approximated by a low-output mass model [see Fig. 8(b)], whereby the unsprung mass is given by the freely moving links. The relation between motor speed (input) and joint position can be accurately captured by a linear model. This allows us to use standard controller design tools such as a linear quadratic regulator (LQR) to design a high-performance joint position controller [53]. The joint position controller is tuned to actively suppress natural oscillations of the unloaded leg. It has a closed-loop bandwidth of around 9 Hz, again depending on the amplitude. It turns out that LQR-based position control leads to a significantly better control performance than a cascaded setup with an inner torque loop (see Section IV-C1) and an outer position loop, which is typically implemented for stiff systems [63].

3) Relation to Existing Solutions: The resulting torque and position control bandwidth is poor, compared with stiff systems with torque sensors, yet they are still within the range of Pratt's benchmarking electrical SEAs ($5-25$ Hz [77]) and above the frequency range that is typically found in human motion ($4-8$ Hz [78]).

V. Experimental Results

The capabilities of Starl*ETH* were extensively tested and validated. We address the four design objectives *versatility*, *speed*, *efficiency*, and *robustness* by presenting various experiments spanning the range of static walking to dynamic running. This demonstrates the applicability of our quadrupedal platform and the underlying control principles. For illustration, all experiments are documented in a movie[5](the individual segments are listed in Table III in the Appendix).

A. Versatility

First of all, Starl*ETH* is capable of different gaits (see Fig. 9) such as static walking (a), a walking trot (b), or a fast running trot (c) with a substantial flight phase, bounding (d), or pronking (e). It can automatically and smoothly switch among the different gaits by interpolating between the subsequent gait graphs (movie segment 4) [71].

Second, our robot is not only suited to locomote on flat ground. Using reactive control techniques, it can cope with unperceived and slippery obstacles, while applying static and dynamic gaits (see also Fig. 12(a) and movie segment 5). Thereby, Starl*ETH* detects ground contact using the pressure sensors, estimates potential slippage by combining kinematic information with IMU measurements [66] and reacts by an appropriate choice of the successive foothold location and contact force distribution. To avoid jitter (high-frequent control phase changes due to rapidly changing contact situations), the controller accounts for a filtered contact force signal, as well as for the demand control phase of the high-level behavior planner.

Furthermore, Starl*ETH* can optimally exploit the redundant contact points for climbing maneuvers (see Fig. 10, movie segment 3). Using the force optimization strategy based on Section IV-B2 and knowledge about the terrain geometry, the contact forces are aligned with the local surface normal direction to minimize the risk of slippage. This allows us to significantly reduce the required friction coefficient and, hence, to safely walk over uneven (but) known surface [79]. In all these experiments, we kept the contact force distribution objective at a lower priority than the motion (see also [73]).

Finally, to achieve fully autonomous operation, Starl*ETH* must be able to carry equipment for perception and processing, as well as batteries for a long energy autonomy. One of the most demanding static maneuvers with respect to required joint torque is standing up from a completely crouched position. We tested Starl*ETH* with a maximal payload of 25 kg, which is about the total weight of the actual robot and a considerably better payload to body weight ratio than for systems such as Little Dog [5], ALoF [6], or large machines like HyQ [14].

B. Speed

With the current control setup, Starl*ETH* is able to robustly trot with a speed of up to $0.7\,\mathrm{m/s}$ respectively 1.5 bodylengths/s. At higher velocities, the robot cannot be reliably stabilized with the current control setup. Given a maximal joint angle velocity of about $10\,\mathrm{rad/s}$ and a nominal leg length of $l = 0.33\,\mathrm{m}$, a locomotion speed of about $2\,\mathrm{m/s}$ is theoretically possible with a typical sinusoidal hip motion (duty factor 0.5). A possibility to overcome this deficiency is to explore high-dynamic running gaits with a smaller duty factor such as running trot [see Fig. 9(c)] or bounding [see Fig. 9(d)] [80].

C. Efficiency

To quantify the overall energy consumption, we performed a series of (control and power) autonomous long-term locomotion experiments with different gaits and speeds. Starl*ETH* was operated with an onboard PC and two 5 Ah 22.2-V LiPo batteries with a total weight of 1.5 kg, which provides operation time of about 1 h. We independently measured energy consumption at the motor controllers, sensor boards, and onboard computer.

[5]http://youtu.be/4ZbifH0Mv4w.

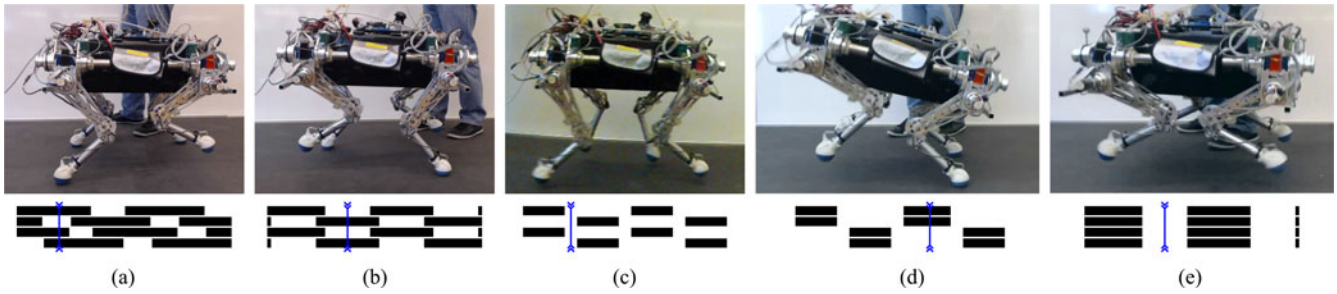

Fig. 9. Starl*ETH* is capable of various gaits such as (a) static walk, (b) walking trot, (c) running trot, (d) bound, or (e) pronk. The blue line indicates the current phase in the gait graph.

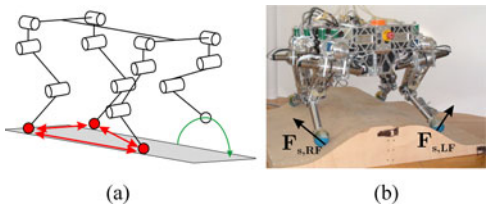

Fig. 10. By exploiting the internal contact directions (a) and aligning the contact forces with the local surface normal directions (b), Starl*ETH* is capable of walking on curved surfaces (adapted from [79]).

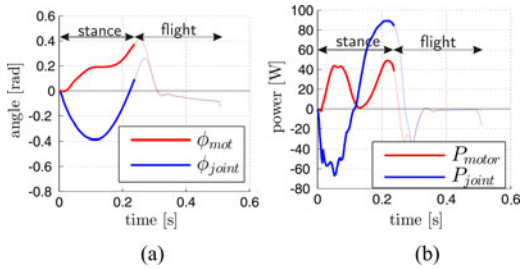

Fig. 11. Position (a) and power (b) courses in the left front knee joint during pronking experiments while exploiting the system's passive dynamics (adapted from [81]).

TABLE II
DETAILED MEASUREMENTS OF ENERGY CONSUMPTION OF THE INDIVIDUAL COMPONENTS

			onb. PC [W]	sensor boards [W]	motor ctrl [W]	total power [W]	total COT [-][a]	elect. loss [-]	corr. COT [-][b]
unloaded			29	16.5	27.6	73.1			
standing			29	16.5	43.9	89.4			
walking	0	m/s	29	16.5	105	150	∞	49%	∞
	0.13	m/s			105	151	4.5	49%	2.3
	0.19	m/s			128	173	3.5	42%	2.0
trotting	0	m/s	29	16.5	109	154	∞	47%	∞
	0.11	m/s			109	154	5.4	47%	2.8
	0.22	m/s			119	164	2.8	44%	1.6
	0.38	m/s			175	220	2.2	33%	1.4
	0.5	m/s			177	223	1.7	33%	1.1

[a]total COT $= \frac{\text{total power}}{m_{tot} \cdot g \cdot v}$.
[b]corr. COT $= \frac{\text{motor ctrl}}{m_{tot} \cdot g \cdot v}$.

All results are summarized in Table II. It is evident that the energy consumption depends on the gait and increases with speed, while the overall COT ($= \frac{P}{m \cdot g \cdot v}$) can be reduced for fast trotting down to 1.7. The detailed analysis of how much the individual components consume unveils another interesting finding. In the setup of Starl*ETH*, third to half of the energy is solely used to power the electronic components. In fact, when considering only the electric power required for actuation, the COT reduces to about 1.1.

SEA have the large potential of mechanically storing and releasing substantial amount of energy in the springs [53]. However, due to the fixed spring stiffness of SEAs, these advantages can only be exploited if the natural dynamics are optimally excited. To demonstrate this ability, Starl*ETH* was controlled to perform a pronking gait [see Fig. 9(e)] with all four legs in simultaneous contact phase. Due to the large vertical oscillation of the main body, this belongs to the most demanding gaits for the joint actuators. To excite this gait respectively the underlying passive oscillation, we actuate the knee joints during stance phase in a feedforward manner by thrusting the motors while stabilization is ensured by the hip actuators [81]. As indicated in Fig. 11(a), the knee joint (blue) undergoes a large motion with a deceleration phase until mid-stance and a slightly longer acceleration phase before lift-off. Thereby, the motor (red) makes a much shorter travel distance by directly going from landing to lift-off configuration. This has a beneficial impact on the power curve, as the motor in Fig. 11(b) produces exclusively positive power throughout the entire stance phase, while the joint first decelerates (energy is stored in the spring) and then reaccelerates again. In fact, the relation between the positive power the motor produces and the positive power the joint actually needs

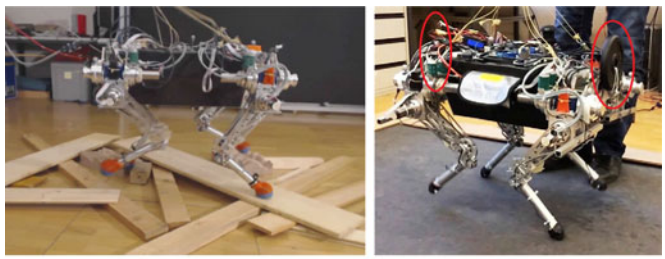

Fig. 12. Starl*ETH* can robustly trot over rough terrain with loose and slippery obstacles (a) and is able to handle certain modeling errors such as unknown payload (b).

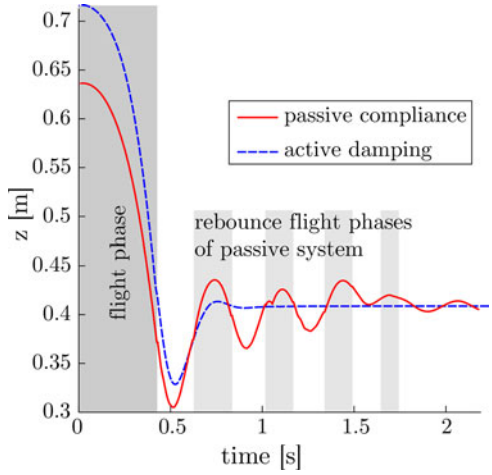

Fig. 13. Vertical main body position of the system dropped from $\approx 0.5\,\mathrm{m}$. The red-dotted curve shows the high oscillations due to the passive compliance with intermittent flight phases (gray area), while active damping (blue-solid) using virtual model control ensures nearly critical damping of the system [1] (picture adapted from [1]).

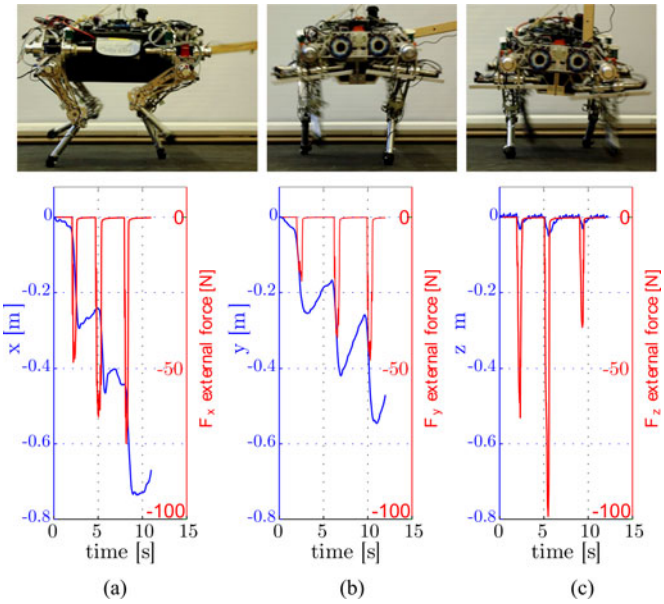

Fig. 14. External pushes applied from different sides while tracking the body motion (blue) and measuring the pushing force (red). (a) Frontal push. (b) Side push. (c) Top push.

to maintain the pronking gait is only about 58%. The rest is passively stored and released by the SEA. The second benefit is that the peak power at the joint of almost $100\,\mathrm{W}$ is a factor two higher than at the motor with less than $50\,\mathrm{W}$.

D. Robustness

The robot must be robust in two contexts. First, the system must be built mechanically robust to reliably work and sustain large impact forces in high-dynamic maneuvers. Second, it must be controlled robustly to cope with different types of disturbances.

1) Mechanical Robustness: Legged systems should softly and safely interact with their environment to protect the hardware from damage through collisions during highly dynamic maneuvers. In particular, stiff systems with electric actuation cannot cope with such situations at all (e.g., [5] and [6]) and largely suffer from the impulsive forces at impacts that harm the gearboxes or the force/torque sensors. In contrast with, decoupling the link and actuator in Starl*ETH* by springs ensures inherent robustness, as impulsive forces are low-pass filtered and only lead to a gradually increasing spring deflection respectively motor output torque. To demonstrate this, Starl*ETH* is dropped from double its standing height (approx. $0.7\,\mathrm{m}$) (movie segment 2). If all motors are blocked, the springs lead to large oscillations (red-solid line in Fig. 13), including a number of short rebounds (gray background) after landing. These oscillations can be actively damped (blue-dashed line in Fig. 13) using a virtual force controller at the main body as explained in Section IV-B1. In this experiment, the desired body position is given by the default standing height at the point of impact, and the target orientation, velocity, and angular velocity are set to be zero. The proportional ($k_p = 600\,\mathrm{N/m}$) and damping gains ($k_d = 10\,\mathrm{Ns/m}$) are tuned to ensure a smooth, overcritically damping behavior.

Mechanical robustness additionally means to ensure reliable and high-endurance operation also under control failure or peak loads. The presented design principles have proven to be a good choice: after two years of almost daily operation, several autonomous endurance ($>1\,\mathrm{km}$, $>1\,\mathrm{h}$) and performance evaluation test as explained in Section V-D1), not a single critical part has been damaged. For safety purpose, the chain was designed to be the weakest mechanical element in the drive train and, hence, breaks in case of an overload when the controller fails. Such mechanical failure happens every couple months but can be quickly ($<5\,\mathrm{min}$) and cheaply ($<2\,\$$) repaired.

2) Control Robustness: The system must be robust against external disturbances (i.e., pushes/pulls or unexpected ground elevations) and internal disturbances (i.e., modeling errors or sensor/actuator inaccuracies). Control robustness can be analytically determined for static walking gaits by the maximal force that leads to tipping over. However, for dynamically stable gaits, robustness is mainly characterized by how well the robot can produce reaction forces and how fast the reflexes are to place the feet accordingly. Since our setup is based on a single centralized computer running at high frequency, there is no need for local reflexes as, e.g., in animals but all feedback loops can be closed over the main controller. However, due to the complexity of the machine and the high number of parameters that influence the overall robustness, we have to rely on experimental evaluations of typical disturbance scenarios.

The most common external disturbances are unperceived and slippery ground obstacles that require redistribution of the contact forces and reactive foot stepping as a function of the desired and actual main body motion (see Fig. 12(a), movie segment 5). As this is hard to quantify, we conducted additional tests with pushing the robot from different sides (front, side, top), while executing a dynamic trotting gait (see Fig. 14, movie segment 9).

During these experiments, we recorded the pushing force using a three-axis force sensor (Optoforce), as well as the body position/orientation using the external motion capture system. As indicated in Fig. 14(a)–(c), forces up to 100 N for about 0.8 s in average can be well compensated by appropriate side stepping and adaptation of reaction forces.

Internal disturbances mostly originate from imprecise modeling, for example, through additional sensor equipment or batteries that are mounted to the main body without adapting control parameters. For evaluation, we kept all control parameters constant (no adaptation and no integrator behavior), while adding external load to the main body [see Fig. 12(b)]. Up to 5 kg payload (which corresponds to 38% of the main body mass), the robot behavior does not change remarkably. With more (unknown) payload, the modeling errors become too large, and the robot starts to slightly stagger.

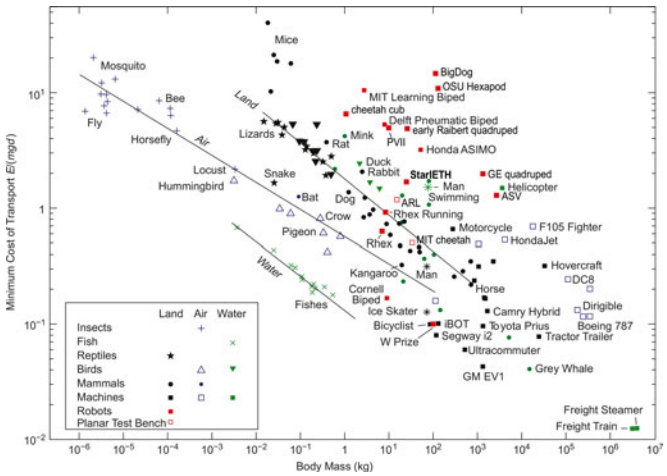

Fig. 15. Comparison of minimum COT as function of body mass for a variety of robots, animals, and vehicles. This picture is adopted from [15] with additional input from [10], [21], [25], and [39].

VI. Conclusion

This paper provides an overview about Starl*ETH*: an autonomous quadrupedal robot that was developed toward combining *fast*, *efficient*, *versatile*, and *robust* locomotion skills in a single device. This system is driven by highly compliant series elastic actuation that makes it fully torque controllable, robust against impacts, and, hence, well suited for dynamic maneuvers. We outlined two model-based control principles and validate the performance of our system in various experiments.

The proposed combination of system design, actuation, and control principles appears to be *versatile* in a sense that the robot is able to execute different gaits that range from static walking to dynamic gaits such as trotting, bounding, or pronking over different types of terrains with unperceived obstacles. These periodic gaits are complemented by a set of special maneuvers (e.g., standing up, squat jumping, etc.) which are possible due to the large range of motion in all joints.

To *robustly* walk on uneven ground and to perform dynamic gaits under significant disturbances from irregular ground or external pushes, Starl*ETH* can simultaneously optimize its motion, the contact forces, and joint torque distribution. While robustness against external pushes was experimentally quantified for comparison with other systems, clear measures of robustness against unperceived terrain elevations (e.g., standardized and scalable terrain samples) are not yet available and need to be defined in the future. Although, hard to quantify, the mechanical compliance seems to help by naturally smoothing the contact forces, which avoids problems of fast contact switches or immediate changes in the contact force and joint torque distribution. Our experience has shown that one of the most critical elements for robust locomotion over irregular ground is a reliable ground contact detection. Since most off-the-shelf force/torque sensors are inapplicable due to their high weight and low impact tolerance, we iterated through several custom made solutions based on force sensing resistors [1], integrated strain gauges [82], contact force estimation from joint torque measurements, and the currently used pressure-based solution [63]. Furthermore, from a design aspect, it turned out to be very useful to mechanically protect all critical elements (e.g., gearbox) by integrating a well-defined breaking point that allows fast and cheap maintenance of the systems even in case of failure. In the current control setup, the leg follows the same swing trajectory to the new stance location until it encounters ground contact. To further enhance robustness and to additionally avoid tripping after hitting an obstacle during swing phase, it will be necessary to implement reflex-like behaviors to adapt the swing phase accordingly [83].

In its presented configuration, Starl*ETH* can be operated autonomously (movie segment 10) with an onboard PC and batteries. Thereby, it has an average energy consumption of less than 230 W and a battery autonomy of about 1 h. We have experimentally shown how the choice of gait and locomotion speed influences the COT. For the range of speed, we were able to cover with our system; we encounter a continuous decrease and not a clear minimum in COT, as it is expected from animals [84], conceptual model [57], or experiments with small-scale robots [39]. A possible reason could be the comparably low locomotion speed of Starl*ETH*. However, further investigations are required to analyze the influence of terrain properties and gait characteristics such as the main body motion or duty factor. Fig. 15 compares the COT of a trotting gait with respect to other documented robots, animals, and wheeled vehicles. Please notice that this comparison has to be made with utmost care as it lists very different types of robots. This ranges from simple planar test bench setups, whereby the actuators are only required to support the body (with minimal stabilization action) (e.g., [25] and [10]), over robots that have external computation or power supply (e.g., [39]), to fully autonomous systems like the Cornell Ranger [21] or Starl*ETH*. Furthermore, *energetic efficiency* is often differently quantified as some people just account for mechanical output power or neglect all electrical energy dissipation in the electronic computation and sensing equipment

TABLE III
DESCRIPTION AND LINK OF INDIVIDUAL MOVIE SEGMENTS

Nr	time	description
1	0 min 04 s	robustness evaluation in dropdown
2	0 min 21 s	different leg configurations
3	0 min 38 s	static walk on uneven ground
4	0 min 57 s	gait transition
5	1 min 06 s	dynamic trotting over obstacles
6	1 min 28 s	pronking over obstacles
7	1 min 38 s	running trot
8	1 min 48 s	bounding
9	2 min 01 s	trotting under external pushes
10	2 min 20 s	autonomous outdoor operation

(see also the discussion in [85]). As we have shown in a detailed analysis summarized in Table II, electrical losses already largely influence this measure.

In terms of *speed*, the presented quadrupedal robot can be robustly stabilized at a locomotion velocity of up to $v_n = 0.7\,\mathrm{m/s}$. Using the nominal leg length of $l_n = 0.33\,\mathrm{m}$ while walking, this corresponds to a Froude number of about $Fr = \frac{v_n^2}{g \cdot l_n} = 0.15$. This is relatively low if compared with the current state of the art and particularly when compared with smaller devices [39]. The higher the locomotion speed, respectively the closer the actuators are to their performance limitation, the more important it becomes to exploit self-stabilization effects and, hence, to propel the system to a large extent using feed forward actuation [57]. Hence, to improve speed, our future work is targeted to use machine learning algorithms for an online optimization of the gait and control parameters [80]. With this, we expect to excite high-dynamic gaits, while optimizing self-stability. Another approach to overcome the limitations of SEAs is to build upon stronger motors and reduced gearbox ratios [9].

In summary, the presented robot Starl*ETH* does not set world records with respect to speed, efficiency, robustness, or versatility but is a strong mixture of all properties pushing the state of the art in autonomous, electrically driven, and torque controllable quadrupedal systems with the potential of being applied in real-world scenarios. Starl*ETH* currently works blindly by haptically detecting the ground contact situation and reacting accordingly. Our future research includes integration of perception capabilities such as laser or vision sensors to improve the state estimation, as well as to establish a map of the local environment. This will be a critical component to enable truly autonomous operation in highly unstructured and unknown real-world environment.

APPENDIX

The supporting movie that is available at this link (http://youtu.be/4ZbifH0Mv4w) consists of the experiments cited in Table III.

REFERENCES

[1] M. Hutter, C. Gehring, M. Bloesch, M. H. Hoepflinger, C. D. Remy, and R. Siegwart, "StarlETH: A compliant quadrupedal robot for fast, efficient, and versatile locomotion," in *Proc. Int. Conf. Climbing Walking Robots*, 2012, pp. 483–490.

[2] Y. Sakagami, R. Watanabe, C. Aoyama, S. Matsunaga, N. Higaki, and K. Fujimura, "The intelligent ASIMO: System overview and integration," in *Proc. Int. Conf. Intell. Robots Syst.*, 2002, vol. 3, pp. 2478–2483.

[3] R. Tajima, D. Honda, and K. Suga, "Fast running experiments involving a humanoid robot," in *Proc. IEEE Int. Conf. Robot. Autom.*, 2009, pp. 1571–1576.

[4] H. Hirukawa, S. Kajita, F. Kanehiro, K. Kaneko, and T. Isozumi, "The human-size humanoid robot that can walk, lie down and get up," *Int. J. Robot. Res.*, vol. 24, no. 9, pp. 755–769, 2005.

[5] M. P. Murphy, A. Saunders, C. Moreira, A. A. Rizzi, and M. Raibert, "The littledog robot," *Int. J. Robot. Res.*, vol. 30, pp. 145–149, 2010.

[6] C. D. Remy, O. Baur, M. Latta, A. Lauber, M. Hutter, M. H. Hoepflinger, C. Pradalier, and R. Siegwart, "Walking and crawling with ALoF: A robot for autonomous locomotion on four legs," *Ind. Robot: Int. J.*, vol. 38, no. 3, pp. 264–268, 2011.

[7] R. Hodoshima, Y. Fukuda, T. Doi, S. Hirose, T. Okamoto, and J. Mori, "Development of TITAN XI: A quadruped walking robot to work on slopes," in *Proc. IEEE/RSJ Int. Conf. Intell. Robots Syst.*, 2004, pp. 792–797.

[8] J. Buchli, M. Kalakrishnan, M. Mistry, P. Pastor, and S. Schaal, "Compliant quadruped locomotion over rough terrain," in *Proc. IEEE/RSJ Int. Conf. Int. Robots Syst.*, 2009, pp. 814–820.

[9] S. Seok, A. Wang, D. Otten, and S. Kim, "Actuator design for high force proprioceptive control in fast legged locomotion," in *Proc. IEEE/RSJ Int. Conf. Intell. Robots Syst.*, 2012, pp. 1970–1975.

[10] S. Seok, A. Wang, D. Otten, J. Lang, and S. Kim, "Design principles for highly efficient quadrupeds and implementation on the MIT Cheetah robot," in *Proc. IEEE Int. Conf. Robot. Autom.*, 2013, pp. 3307–3312.

[11] J. M. Hollerbach, I. W. Hunter, and J. Ballantyne, "A comparative analysis of actuator technologies for robotics," *Robot. Rev.*, vol. 2, pp. 299–342, 1991.

[12] M. Raibert, K. Blankespoor, G. Nelson, and R. Playter, "BigDog, the rough-terrain quadruped robot," in *Proc. 17th World Congr.*, 2008, pp. 10823–10825.

[13] Boston Dynamics. (2012). [Online]. Available: http://www.bostondynamics.com 2012.

[14] C. Semini, N. G. Tsagarakis, E. Guglielmino, M. Focchi, F. Cannella, and D. G. Caldwell, "Design of HyQ—A hydraulically and electrically actuated quadruped robot," *Inst. Mech. Eng., Part I, J. Syst. Control Eng.*, vol. 225, no. 6, pp. 831–849, 2011.

[15] A. Kuo, "Choosing your steps carefully: Trade-offs between economy and versatility in dynamic walking bipedal robots," *IEEE Robot. Autom. Mag.*, vol. 14, no. 2, pp. 18–29, Jun. 2007.

[16] A. Ruina and J. Cortell, "Homepage of Cornell Ranger, 2011, 4-legged bipedal robot," 2011.

[17] S. H. Collins, and A. Ruina, "A bipedal walking robot with efficient and human-like gait," in *Proc. IEEE Int. Conf. Robot. Autom.*, 2005, pp. 1983–1988.

[18] J. M. Donelan, R. Kram, and A. D. Kuo, "Mechanical work for step-to-step transitions is a major determinant of the metabolic cost of human walking," *J. Exp. Biol.*, vol. 205, no. Pt 23, pp. 3717–3727, 2002.

[19] R. M. Alexander, *Principles of Animal Locomotion*. Princeton, NJ, USA: Princeton Univ. Press, 2003.

[20] T. McGeer, "Passive dynamic walking," *Int. J. Robot. Res.*, vol. 9, no. 2, pp. 62–82, 1990.

[21] P. A. Bhounsule, J. Cortell, and A. Ruina, "Design and control of ranger: An energy-efficient, dynamic walking robot," in *Proc. Int. Conf. Climbing Walking Robots*, pp. 441–448, 2012.

[22] G. A. Cavagna, F. P. Saibene, and R. Margaria, "Mechanical work in running," *J. Appl. Physiol.*, vol. 19, no. 2, pp. 249–256, 1964.

[23] R. M. Alexander, "3 uses for springs in legged locomotion," *Int. J. Robot. Res.*, vol. 9, no. 2, pp. 53–61, 1990.

[24] M. H. Raibert, *Legged Robots That Balance*. Cambridge, MA, USA: MIT Press, 1986.

[25] P. Gregorio, M. Ahmadi, and M. Buehler, "Design, control, and energetics of an electrically actuated legged robot," *IEEE Trans. Syst., Man, Cybern. Part B, Cybern.*, vol. 27, no. 4, pp. 626–634, Aug. 1997.

[26] H. D. Taghirad, "*Analysis, design, and control of hopping robot*," Master thesis, McGill University, Montreal, QC, Canada, 1993.

[27] M. Ahmadi and M. Buehler, "Controlled passive dynamic running experiments with the ARL-monopod II," *IEEE Trans. Robot.*, vol. 22, no. 5, pp. 974–986, Oct. 2006.

[28] M. D. Berkemeier and K. V. Desai, "Design of a robot leg with elastic energy storage, comparison to biology, and preliminary experimental results," in *Proc. IEEE Int. Conf. Robot. Autom.*, 1996, pp. 213–218.

[29] H. De Man, D. Lefeber, and J. Vermeulen, "Design and control of a robot with one articulated leg for locomotion on irregular terrain," in *CSIM Courses and Lectures*, New York, NY, USA: Springer, vol. 405, ch. VI, 1998, pp. 417–424.

[30] S. H. Hyon and T. Mita, "Development of a biologically inspired hopping robot-Kenken,' " in *Proc. IEEE Int. Conf. Robot. Autom.*, 2002, pp. 3984–3991.

[31] J. G. Nichol and K. J. Waldron, "Biomimetic leg design for untethered quadruped gallop," in *Proc. Int. Conf. Climbing Walking Robots*, 2002.

[32] L. R. Palmer, D. E. Orin, D. W. Marhefka, J. P. Schmiedeler, and K. J. Waldron, "Intelligent control of an experimental articulated leg for a galloping machine," in *Proc. IEEE Int. Conf. Robot. Autom.*, 2003, pp. 3821–3827.

[33] S. Curran and D. E. Orin, "Evolution of a jump in an articulated leg with series-elastic actuation," in *Proc. IEEE Int. Conf. Robot. Autom.*, 2008, pp. 252–258.

[34] J. W. Hurst, "The role and implementation of compliance in legged locomotion," Ph.D. dissertation, Robotics Inst., Carnegie Mellon Univ., Pittsburgh, PA, USA, 2008.

[35] J. A. Grimes and J. W. Hurst, "Design of ATRIAS 1.0 A unique monopod, hopping robot," in *Proc. Int. Conf. Climbing Walking Robots*, pp. 548–554, 2012.

[36] J. G. Nichol, S. P. N. Singh, K. J. Waldron, L. R. Palmer III, D. E. Orin, and L. R. Palmer, "System design of a quadrupedal galloping machine," *Int. J. Robot. Res.*, vol. 23, no. 10/11, pp. 1013–1027, 2004.

[37] I. Poulakakis, J. A. Smith, and M. Buehler, "Modeling and experiments of untethered quadrupedal running with a bounding gait: The Scout II robot," *Int. J. Robot. Res.*, vol. 24, no. 4, pp. 239–256, 2005.

[38] H. Kimura, Y. Fukuoka, and A. H. Cohen, "Adaptive dynamic walking of a quadruped robot on natural ground based on biological concepts," *Int. J. Robot. Res.*, vol. 26, no. 5, pp. 475–490, 2007.

[39] A. Sprowitz, A. Tuleu, M. Vespignani, M. Ajallooeian, E. Badri, and A. J. Ijspeert, "Towards dynamic trot gait locomotion: Design, control, and experiments with Cheetah-cub, a compliant quadruped robot," *Int. J. Robot. Res.*, vol. 32, no. 8, pp. 932–950, 2013.

[40] F. Iida, G. Gomez, and R. Pfeifer, "Exploiting body dynamics for controlling a running quadruped robot," in *Proc. Int. Conf. Robot. Autom.*, 2005, pp. 229–235.

[41] G. A. Pratt and M. M. Williamson, "Series elastic actuators," in *Proc. IEEE Int. Conf. Intell. Robots Syst.*, 1995, pp. 399–406.

[42] J. Pratt, B. Krupp, and C. Morse, "Series elastic actuators for high fidelity force control," *Ind. Robot: Int. J.*, vol. 29, no. 3, pp. 234–241, 2002.

[43] M. Slovich, N. Paine, K. Kemper, A. Metger, A. Edinger, J. Weber, and L. Sentis, "Building HUME: A bipedal robot for human-centered hyperagility," in *Proc. Dyn. Walking Meeting*, 2012.

[44] K. Radkhah, C. Maufroy, M. Maus, Scholz D, A. Seyfarth, and O. Von Stryk, "Concept and design of the biobiped1 robot for human-like walking and running," *Int. J. Humanoid Robot.*, vol. 8, no. 3, pp. 439–458, 2011.

[45] N. Tsagarakis and Z. Li, "The design of the lower body of the compliant humanoid robot 'cCub,' " in *Proc. IEEE Int. Conf. Robot. Autom.*, 2011, pp. 2035–2040.

[46] J. Pratt and B. Krupp, "Design of a bipedal walking robot," in *Unmanned Systems Technology X*, pp. 69621F-1–69621F-13, 2008.

[47] P. G. Gonzales de Santos, E. Garcia, and J. Estremera, "Stability in walking robots," in *Quadrupedal Locomotion. An Introduction to the Control of Four-legged Robots*, vol. 1, Berlin, Germany: Springer, 2006, pp. 33–54.

[48] J. Pratt, C.-M. Chew, A. Torres, P. Dilworth, and G. Pratt, "Virtual model control: An intuitive approach for bipedal locomotion," *Int. J. Robot. Res.*, vol. 20, no. 2, pp. 129–143, 2001.

[49] L. Sentis and O. Khatib, "Control of free-floating humanoid robots through task prioritization," in *Proc. IEEE Int. Conf. Robot. Autom.*, 2005, pp. 1718–1723.

[50] R. Philippsen, L. Sentis, O. Khatib, and L. Sentist, "An open source extensible software package to create whole-body compliant skills in personal mobile manipulators," in *Proc. IEEE/RSJ Int. Conf. Intell. Robots Syst.*, 2011, pp. 1036–1041.

[51] M. Mistry, J. Buchli, and S. Schaal, "Inverse dynamics control of floating base systems using orthogonal decomposition," in *Proc. Int. Conf. Robot. Autom.*, 2010, pp. 3406–3412.

[52] L. Righetti, J. Buchli, M. Mistry, M. Kalakrishnan, and S. Schaal, "Optimal distribution of contact forces with inverse-dynamics control," *Int. J. Robot. Res.*, vol. 32, no. 3, pp. 280–298, 2013.

[53] M. Hutter, C. D. Remy, M. A. Hoepflinger, and R. Siegwart, "Efficient and versatile locomotion with highly compliant legs," *IEEE/ASME Trans. Mechatronics*, vol. 18, no. 2, pp. 449–458, Apr. 2013.

[54] C. Semini, "HyQ—Design and development of a hydraulically actuated quadruped robot," Ph.D. dissertation, Univ. Genoa, Genoa, Italy, 2010.

[55] M. Hutter, C. D. Remy, M. H. Hoepflinger, and R. Siegwart, "High compliant series elastic actuation for the robotic leg ScarlETH," in *Proc. Int. Conf. Climbing Walking Robots*, Paris, France, 2011, pp. 507–514.

[56] P. Chatzakos and E. Papadopoulos, "The influence of DC electric drives on sizing quadruped robots," in *Proc. IEEE Int. Conf. Robot. Autom.*, 2008, pp. 793–798.

[57] C. D. Remy, *"Optimal expoitation of natrual dynamics in legged locomotion,"* Ph.D. dissertation, ETH Zurich, Zurich, Switzerland, 2011.

[58] C. T. Farley, R. Blickhan, J. Saito, and C. R. Taylor, "Hopping frequency in humans—A test of how springs set stride frequency in bouncing gaits," *J. Appl. Physiol.*, vol. 71, no. 6, pp. 2127–2132, 1991.

[59] N. Paine, S. Oh, and L. Sentis, "Design and control considerations for high-performance series elastic actuators," *IEEE/ASME Trans. Mechatronics*, vol. 19, no. 3, pp. 1080–1091, Jun. 2014.

[60] D. W. Robinson, *"Design and analysis of series elasticity in closed-loop actuator force control,"* Ph.D. dissertation, Mass. Inst. Technol., Cambridge, MA, USA, 2000.

[61] Maxon Motor AG. (2013). EC-4pole 30 datasheet: [Online]. Available: http://www.maxonmotor.ch/medias/sys_master/8807044087838/13_202_EN.pdf

[62] S. Schaal, "The SL simulation and real-time control software package," Univ. Southern Calif., Los Angeles, CA, USA, Tech. Rep., 2009.

[63] M. Hutter, *"StarlETH & co-design and control of legged robots with compliant actuation*," Ph.D. dissertation, ETH Zurich, Zurich, Switzerland, 2013.

[64] M. Hutter, C. Gehring, and R. Siegwart, "proNEu: Derivation of analytical kinematics and dynamics," ETH Zurich, Zurich, Switzerland, Tech. Rep., 2011.

[65] M. Bloesch, M. Hutter, M. Hoepflinger, S. Leutenegger, C. Gehring, C. D. Remy, and R. Siegwart, "State estimation for legged robots—Consistent fusion of leg kinematics and IMU," in *Proc. Robot. Sci. Syst.*, 2012, pp. 17–24.

[66] M. Bloesch, C. Gehring, P. Fankhauser, M. Hutter, M. A. Hoepflinger, and R. Siegwart, "State estimation for legged robots on unstable and slippery terrain," in *Proc. IEEE/RSJ Int. Conf. Intell. Robots Syst.*, 2013, pp. 6058–6064.

[67] C. Gehring, G. Nuetzi, R. Diethelm, R. Siegwart, and R. I. Leine, "An evaluation of Moreau's time-stepping scheme for the simulation of a legged robot," presented at the ASME Int. Design Eng. Tech. Conf., Buffalo, New York, USA, 2014.

[68] R. B. McGhee, A. A. Fkask, and A. Frank, "On the stability properties of quadruped creeping gaits," *Math. Biosci.*, vol. 3, pp. 331–351, Aug. 1968.

[69] P. D. Neuhaus, J. E. Pratt, and M. J. Johnson, "Comprehensive summary of the institute for human and machine cognition's experience with LittleDog," *Int. J. Robot. Res.*, vol. 30, no. 2, pp. 216–235, 2011.

[70] J. E. Pratt and R. Tedrake, "Velocity-based stability margins for fast bipedal walking," in *Fast Motions in Biomechanics and Robotics*. Berlin, Germany: Springer, 2006, pp. 299–324.

[71] C. Gehring, S. Coros, M. Hutter, M. Bloesch, M. A. Hoepflinger, and R. Siegwart, "Control of dynamic gaits for a quadrupedal robot," in *Proc. IEEE Int. Conf. Robot. Autom.*, 2013, pp. 3287–3292.

[72] S. Coros, A. Karpathy, B. Jones, L. Reveret, and M. van de Panne, "Locomotion skills for simulated quadrupeds," *ACM Trans. Graph.*, vol. 30, no. 4, pp. 59:1–59:12, 2011.

[73] M. Hutter, H. Sommer, C. Gehring, M. Hoepflinger, M. Bloesch, and R. Siegwart, "Quadrupedal locomotion using hierarchical operational space control," *Int. J. Robot. Res.*, vol. 33, pp. 1062–1077, May 2014.

[74] A. Bjoerck, *Numerical Methods for Least Squares Problems*. Philadelphia, PA, USA: SIAM, 1996.

[75] G. A. Pratt, P. Willisson, C. Bolton, and A. Hofman, "Late motor processing in low-impedance robots: Impedance control of series-elastic actuators," in *Proc. Amer. Control Conf.*, 2004, vol. 4, pp. 3245–3251.

[76] E. Colgate and N. Hogan, "An analysis of contact instability in terms of passive physical equivalents," in *Proc. IEEE Int. Conf. Robot. Autom.*, 1989, pp. 404–409.
[77] J. E. Pratt and B. T. Krupp, "Series elastic actuators for legged robots," *Proc. SPIE*, vol. 5422, pp. 135–144, 2004.
[78] K. Kong, J. Bae, and M. Tomizuka, "Control of rotary series elastic actuator for ideal force-mode actuation in human & robot interaction applications," *IEEE/ASME Trans. Mechatronics*, vol. 14, no. 1, pp. 105–118, Feb. 2009.
[79] M. Hutter, M. Hoepflinger, C. D. Remy, and R. Siegwart, "Hybrid operational space control for compliant legged systems," in *Proc. Robot. Sci. Syst.*, pp. 129–136, 2012.
[80] C. Gehring, S. Coros, M. Hutter, M. Bloesch, P. Fankhauser, M. Hoepflinger, and R. Siegwart, "Towards automatic discovery of agile gaits for quadrupedal robots," in *Proc. IEEE Int. Conf. Robot. Autom.*, 2014, pp. 4243–4248.
[81] M. Hutter, C. Gehring, M. Bloesch, M. Hoepflinger, P. Fankhauser, and R. Siegwart, "Excitation and stabilization of passive dynamics in locomotion using hierarchical operational space control," in *Proc. IEEE Int. Conf. Robot. Autom.*, 2014, pp. 2977–2982.
[82] F. Loehr, *"Robust and reliable ground contact sensing for legged robots*," Bachelor thesis, ETH Zurich, Zurich, Switzerland, 2013.
[83] M. Focchi, V. Barasuol, I. Havoutis, J. Buchli, C. Semini, and D. G. Caldwell, "Local reflex generation for obstacle negotiation in quadrupedal locomotion," in *Proc. Int. Conf. Climbing Walking Robots*, 2013, pp. 443–450.
[84] D. F. Hoyt and C. R. Taylor, "Gait and the energetics of locomotion in horses," *Nature*, vol. 292, no. 5820, pp. 239–240, 1981.
[85] M. de Lasa, "*Dynamic compliant walking of the Scout II quadruped*," Master thesis, Montreal, QC, Canada, 2000.

Marco Hutter received the B.Sc. M.Sc. and the Dr.Sc. degrees in mechanical engineering from ETH Zurich, Zurich, Switzerland, in 2007, 2009, and 2013 respectively.

He is currently working as a Senior Scientist with the Autonomous Systems Lab, ETH Zurich. His research interests include legged robotic systems, whereby he is working on system and actuator design, low-level force and position control, as well as on model-based locomotion control.

Christian Gehring received the B.Sc. and M.Sc. degrees in mechanical engineering from ETH Zurich, Zurich, Switzerland, in 2008 and 2011, respectively. He is currently a doctoral student with the Autonomous Systems Lab, ETH Zurich, and closely collaborates with Disney Research Zurich.

His research interests include control of life-like, agile, and robust quadrupedal locomotion. He works on model-based motion control and motion planning to enable various gaits and gait transitions for force-controlled quadrupeds.

Mark A. Höpflinger received the M.Sc. degree in electrical engineering and information technology and the Dr.Sc. degree from ETH Zurich, Zurich, Switzerland, in 2007 and 2013, respectively.

He is currently a Postdoctoral Researcher with the Autonomous Systems Lab, ETH Zurich. His research interests include perception for legged robots.

Michael Blösch received the B.Sc. and M.Sc. degrees in mechanical engineering from ETH Zurich, Zurich, Switzerland, in 2009 and 2012, respectively. He is currently pursuing the Ph.D. degree with the Autonomous Systems Lab, ETH Zurich, where he is working on state estimation and perception for legged robotics.

His research interests include sensor fusion, vision and laser perception, as well as legged locomotion.

Roland Siegwart (F'08) received the Master's and Ph.D. degrees in mechanical engineering from ETH Zurich, Switzerland. He has been a Full Professor of Autonomous Systems and the Vice-President of Research and Corporate Relations, ETH Zurich, Zurich, Switzerland, since 2006 and 2010, respectively. From 1996 to 2006, he was an Associate and later a Full Professor for Autonomous Microsystems and Robots with the Ecole Polytechnique Fédérale de Lausanne, Lausanne, Switzerland.

Prof. Siegwart is Member of the Swiss Academy of Engineering Sciences and a Officer of the International Federation of Robotics Research. He served as the Vice-President for Technical Activities (2004/2005) and was Distinguished Lecturer (2006/2007) and was an AdCom Member (2007–2010) of the IEEE Robotics and Automation Society. He leads a research group of around 30 people working in the fields of robotics, mechatronics, and product design.